Material: Ferritic Steel: F82H
Property: Engineering Stress vs. strain
Condition: Un-irradiated
Data: Experimental
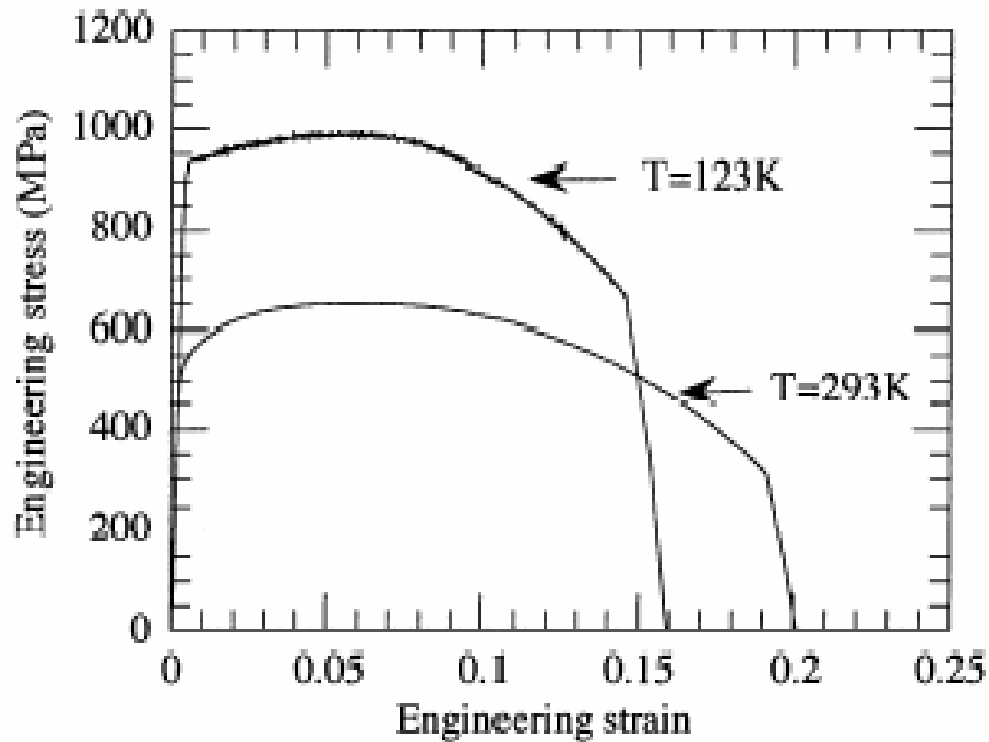

Fig. 1. Engineering stress–engineering strain tensile curves at 123 and 293 K, $\dot{\varepsilon}_p = 2 \times 10^{-3} \, s^{-1}$.
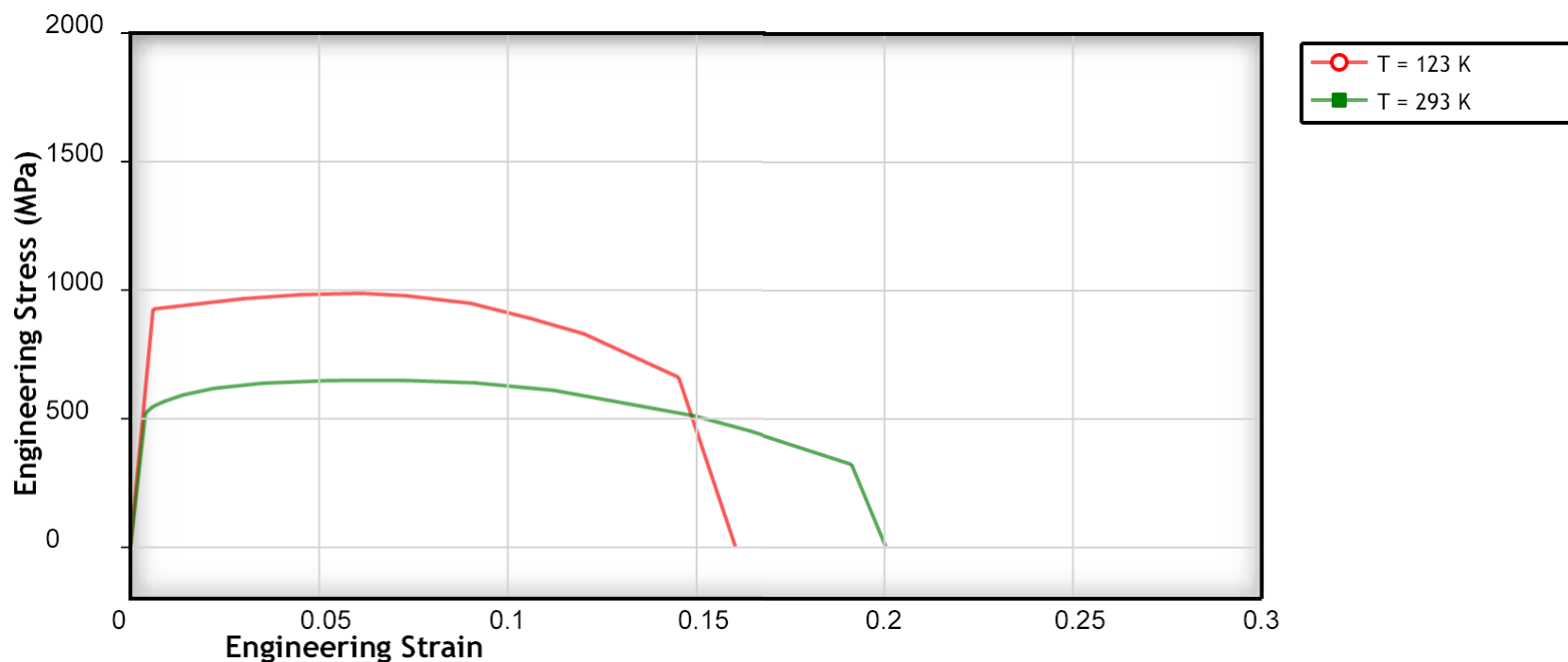
Title of paper (or report) this figure appeared in:
On the Constitutive Behavior of the F82H Ferritic/Martensitic Steel

Author of paper or graph:

P. Spatig, N. Baluc, M. Victoria

Caption:

Engineering stress-engineering strain tensile curves at 123 and 293 K, ε_p = 2 x 10^-3 s^-1.

Engineering stress-engineering strain tensile curves at 123 and 293 K, ε_p = 2 x 10^-3 s^-1.

View Data   Author Comments

Plot Format:

Y-Scale: ⦿ linear ◯ log ◯ ln
X-Scale: ⦿ linear ◯ log ◯ ln

Update   Close Window

On the constitutive behavior of the F82H ferritic/martensitic steel

P. Spätig*, N. Baluc, M. Victoria

*Centre de Recherches en Physique des Plasmas-Technologie de la Fusion, Association Confédération Suisse-Euratom,
Ecole Polytechnique Fédérale de Lausanne, CH-5232 Villigen PSI, Switzerland*

Abstract

This paper focuses on the constitutive behavior of the F82H ferritic/martensitic steels internationally investigated in the frame of the fusion material development program. Tensile tests were carried out in the temperature range (80–723 K) at different strain rates. A decomposition of the flow stress into a yield stress plus a hardening stress component is proposed. The temperature, strain and strain rate dependence of the stress is discussed based on the current available data. The strain-hardening is calculated and two strain-hardening stages are identified along the deformation curves between the yield stress and the necking instability. Finally, semi-empirical constitutive relations, which are partly based on dislocation mechanics, are derived. © 2001 Elsevier Science B.V. All rights reserved.

Keywords: Ferritic/martensitic steel; Stress–strain curve; Dislocation mechanics

1. Introduction

Ferritic/martensitic steels of the 7–9Cr class are potential candidate materials for the first wall and blanket of the future commercial fusion reactors [1,2]. To date, a great deal of studies have been undertaken, in the frame of the international fusion material development program, to investigate and characterize the mechanical properties, the microstructures [3] and their evolution and stability under irradiation [4]. In particular, the tensile properties have been the subject of many investigations mainly to determine the irradiation-induced hardening and the loss of ductility, e.g. [5,6]. However, the general constitutive behavior of these steels, characterizing the relation between the flow stress to the strain rate and temperature, is poorly documented. It must be emphasized that it is of primary importance to develop accurate models for the constitutive relations for predicting defect tolerance in flawed fusion reactor structures. Indeed, finite element modeling has been widely used to model the fracture behavior of the ferritic steels [7] and up to now, the constitutive behavior used in the simulations was usually relations of the Ramberg–Osgood type. However, the Ramberg–Osgood equation or any similar power law relations between stress and strain are only adjusted fits but are not physically based on the mechanics and dynamics of dislocations. In order to have and gain confidence in the results of continuum simulations, it is highly desirable to establish more physically based equations. To address this issue, a series of tensile tests have been done up to failure over a range of temperature (80–723 K) and at different strain rate. The stress–strain curves have been analyzed up to the ultimate tensile stress before necking begins. A general decomposition of the flow stress has been considered and special attention has been paid to the strain-hardening behavior. A description of the entire deformation curve by piecewise-linked segments is proposed where actually only two simple functions are necessary to reconstruct the curve between the yield stress and the necking instability. The goal of the paper is not to present an exhaustive study on the constitutive equations of ferritic/martensitic steels but rather to aim at defining a semi-empirical methodology to describe the deformation behavior.

2. Experimental procedure

The alloy used in this study is the reduced activation F82H steel being investigated as part of an International Energy Agency (IEA) coordinated program on ferritic/martensitic steels. The F82H steel contains 7.65 wt.% Cr, 2 wt.% W and Mn, Mo, V, Ta, Ti, Si and C below 1 wt.% in sum total and Fe for the balance. The steel was heat-treated by normalizing at 1313 K for 0.5 h and tempering at 1013 K for 2 h [8]. The fully martensitic and δ-ferrite free structure obtained after quenching transforms during tempering into the so-called "tempered martensite" structure [9], characterized by prior austenite grain boundaries and tempered martensite laths. A detailed investigation of the microstructure can be found in [10].

* Corresponding author. Tel.: +41-56-310-2934; fax: +41-56-310-4529.
E-mail address: philippe.spatig@psi.ch (P. Spätig).

Tensile tests were performed on round specimens of 3 mm in diameter and 18 mm in gauge length. The tests were carried out on a servo-hydraulic machine at constant nominal strain rates of 2×10^{-4} and $2 \times 10^{-3}\,\mathrm{s}^{-1}$ in the temperature range from 80 to 293 K. The tests were carried out either in a liquid-nitrogen-cooled alcohol bath or regulated N_2 gas environment. In addition, yield stress results obtained on tests at temperatures up to 723 K under vacuum environment at the nominal strain rate of $2.8 \times 10^{-5}\,\mathrm{s}^{-1}$ previously performed at the Paul Scherrer Institute [11] in Switzerland, are also reported in this paper.

3. Results and discussion

In Fig. 1, two typical engineering stress-engineering strain curves at 293 and 123 K are presented. The overall shape of these tensile curves look relatively similar, the flow stress at 123 K being about 360 MPa higher than that at 293 K reflecting mostly the difference in the yield stress. However, small and subtle differences in the shape of the deformation curves could be identified such as, for example, a transition between the elastic domain and the plastic domain more pronounced with decreasing temperature. The strain-hardening rate, defined as $\theta_p = \mathrm{d}\sigma/\mathrm{d}\varepsilon_p$ where σ is the true stress and ε_p is the plastic component of the true strain, decreases monotonously from the yield stress up to the necking instability. In order to investigate the strain-hardening behavior, in terms of temperature and strain rate dependence as well as stages, the overall flow stress σ has been decomposed as

$$\sigma(\varepsilon_p, \dot{\varepsilon}_p, T) = \sigma_y(\dot{\varepsilon}_p, T) + \sigma_{pl}(\varepsilon_p, \dot{\varepsilon}_p, T) \qquad (1)$$

where σ_y is the yield stress, defined at $\varepsilon_p = 0.002$, and σ_{pl} is the hardening component. As expected for bcc materials, σ_y has been previously shown to be strongly temperature and strain-rate dependent [12] in the low temperature domain, i.e. below room temperature. On the contrary, the hardening component σ_{pl}, which is primarily determined by the evolution of the total dislocation density and

reorganization of the microstructure with strain in the material, is expected to be less sensitive to $\dot{\varepsilon}_p$ and T than the yield stress. Fig. 2 shows the normalized yield stress σ_y/μ, where μ is the shear modulus versus a strain-rate compensated temperature T'. T' is defined to correlate $\sigma_y(T, \dot{\varepsilon}_p)$ with $\sigma_y(T', \dot{\varepsilon}_p^r)$ where $\dot{\varepsilon}_p^r$ is a reference strain rate. The relation between T', $\dot{\varepsilon}_p$ and $\dot{\varepsilon}_p^r$ is given by [13]

$$T' = T\left[1 + C\ln\left(\frac{\dot{\varepsilon}_p^r}{\dot{\varepsilon}_p}\right)\right] \qquad (2)$$

For a reference strain rate equal to $2 \times 10^{-4}\,\mathrm{s}^{-1}$, C has been found equal to about 0.042 [13,14]. From the temperature dependence of σ_y/μ three temperature regimes have been identified [12,14]. A strong thermally activated rate controlling mechanism of Peierls type was associated with the temperature regime I corresponding to temperatures below 200 K. In the temperature regime II, between 200 K and room temperature, the yield stress is only weakly thermally activated and other rate controlling mechanisms, competing with the Peierls one are likely to become operative. In the athermal regime III above room temperature, the flow stress is considered to be controlled by discrete dislocation obstacles and interactions between moving and forest dislocations like in FCC materials. In [13], we have proposed a mathematical description of the temperature dependence of the yield stress over the range (80–723 K) by using two separate functions, one below room temperature and one above. Among the data presented in Fig. 2 only those obtained at $\dot{\varepsilon}_p = 2 \times 10^{-3}\,\mathrm{s}^{-1}$ come from plain tensile tests. For the other ones at $\dot{\varepsilon}_p = 2 \times 10^{-4}\,\mathrm{s}^{-1}$ and at $\dot{\varepsilon}_p = 2.8 \times 10^{-5}\,\mathrm{s}^{-1}$, either stress relaxation experiments or strain-rate jumps were performed at the yield stress. These types of transient experiments influence locally the stress–strain curve or the strain-hardening behavior typically over a plastic strain smaller than 0.01. It is then unrealistic to investigate the strain-hardening behavior at low strain levels (<0.01) when such tests have been performed. For this reason, only the tests performed
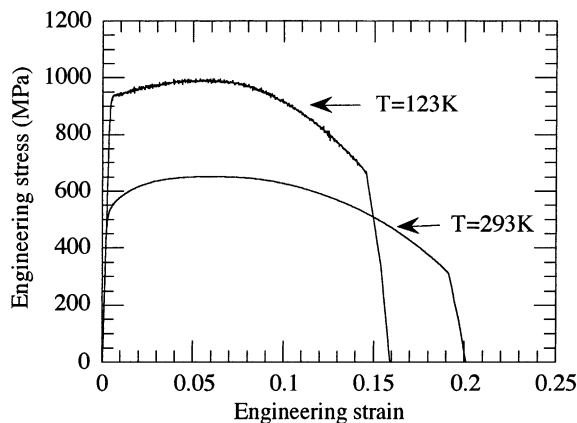
Fig. 1. Engineering stress–engineering strain tensile curves at 123 and 293 K, $\dot{\varepsilon}_p = 2 \times 10^{-3}\,\mathrm{s}^{-1}$.
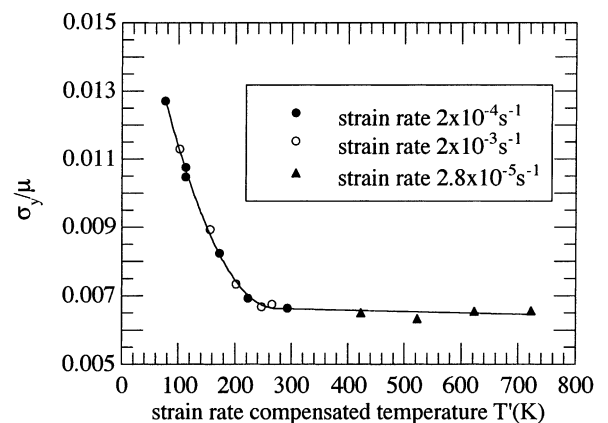
Fig. 2. Strain rate compensated temperature dependence of the normalized yield stress σ_y/μ.
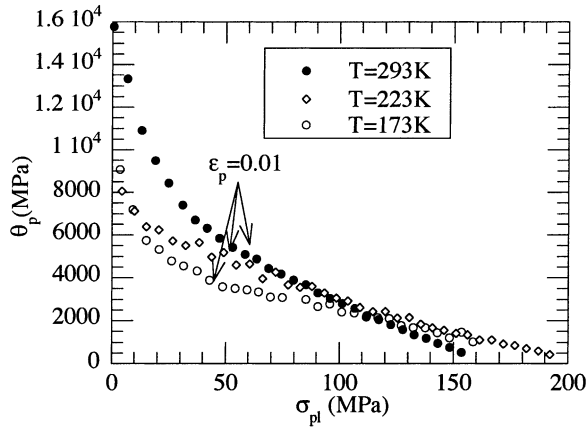
Fig. 3. Strain-hardening rate θ_p vs. the hardening component σ_{pl} at $T = 293$, 223 and 173 K, $\dot{\varepsilon}_p = 2 \times 10^{-3}\,\mathrm{s}^{-1}$.

at $\dot{\varepsilon}_p = 2 \times 10^{-3}\,\mathrm{s}^{-1}$ have been analyzed in terms of the hardening component σ_{pl} in the low strain range.

As an example, the strain-hardening of three curves at 293, 223 and 173 K is plotted against σ_{pl} in Fig. 3. Plotting θ_p versus the true stress is particularly useful to establish an integrated stress–strain law and/or to identify different strain-hardening stages along a deformation curve, e.g [15]. In Fig. 3, it can be seen that the θ_p curves exhibit a sharp decrease in the initial stage of the curves, namely between $\varepsilon_p = 0.002$ and 0.01, while beyond $\varepsilon_p = 0.01$, the decrease is weaker and can be described by a linear function of the stress in a good approximation. For $\varepsilon_p > 0.01$ θ_p is written as

$$\theta_p = \frac{\mathrm{d}\sigma_{pl}}{\mathrm{d}\varepsilon_p} = K_1 - K_2\sigma_{pl} \quad \varepsilon_p \geq 0.01 \tag{3}$$

where the coefficients K_1 and K_2 are in MPa and dimensionless, respectively. Integration of Eq. (3) with the initial condition $\sigma_{pl} = \sigma_{0.01}$ at $\varepsilon_p = 0.01$ yields

$$\sigma_{pl}(\varepsilon_p) = \frac{K_1}{K_2}[1 - \exp[-K_2(\varepsilon_p - 0.01)]]$$
$$+\sigma_{0.01} \quad \varepsilon_p \geq 0.01 \tag{4}$$

This is the equation of the Voce curve [16] starting at $\sigma_{pl} = \sigma_{0.01}$ for $\varepsilon_p = 0.01$ and reaching a saturation stress asymptotically. The saturation stress σ_{sat} is equal to $K_1/K_2 + \sigma_{pl}(0.0\,1)$. Note that the same qualitative behavior for the strain-hardening has been found for temperatures ranging between 80 and 723 K. The temperature effect on the Voce curves and in particular on the coefficients K_1/K_2, K_2 and σ_{sat}, have already been presented and discussed in [13]. Assuming a common fit for the data at different strain rates, namely $\dot{\varepsilon}_p = 2 \times 10^{-3}\,\mathrm{s}^{-1}$ and $\dot{\varepsilon}_p = 10^{-4}\,\mathrm{s}^{-1}$, it has been shown [13] that the logarithms of the $(K_1/K_2)/\mu$, $\sigma_{\mathrm{sat}}/\mu$ and K_2 are linear functions of the dimensionless temperature $kT/\mu b^3$ between 220 and 620 K, b is the amplitude of the Burgers vector. Let us emphasize that even though a temperature dependence of the strain-hardening coefficients

$(K_1/K_2)/\mu$, $\sigma_{\mathrm{sat}}/\mu$ and K_2 could be evidenced and quantified, this dependence remains weak. Hence, the shape and strain-hardening of the deformation curves at different temperatures is not significantly affected by the temperature. The linear fits proposed in [13] were based on the original idea of Kocks [17] who proposed a mechanistic interpretation of the Eq. (4) and applied it to aluminium, copper and stainless steel for which he could fit the midrange of the curves $\theta_p(\sigma)$ with straight lines. Since the strain-hardening is due to the evolution of the dislocation density and rearrangement of the microstructure with strain, the evolution rate of the dislocation density has been attributed to two contributions [17,18,19]. The first one arises from the storage rate of dislocations, which is characterized by their mean free path. The dynamic annihilation of dislocations is responsible for the second contribution. The Eq. (3) reflects actually these two contributions, following Kocks model, K_1 is related to the storage rate or mean free path of the dislocations while K_2 characterizes the dynamic annihilation of dislocations which occurs even at low temperatures [20]. It has been shown that K_1 is proportional to the inverse of the mean dislocation free path L and K_2 is proportional to an average annihilated dislocation length when an annihilation event takes place. In Kocks model, the key structure parameter is the total dislocation density while the detailed microstructure is not explicitly accounted for. Based on that observation, Kocks model appears oversimplified for the type of steel studied in this paper. However, it provides at least some fundamental basis toward the elaboration of a more sophisticated model and K_1 and K_2 can be considered as averaging values lumping together all the effects of the microstructure evolution taking place simultaneously in the laths, the lath boundaries and in the prior austenite grain boundaries. For the tests performed at $\dot{\varepsilon}_p = 2 \times 10^{-3}\,\mathrm{s}^{-1}$, the temperature dependence of the dimensionless coefficients K_1/μ and K_2 is plotted in Fig. 4, where K_1 has been normalized by the temperature dependent shear modulus. Both parameters increase significantly from 123 up to 293 K. Qualitatively, this temperature
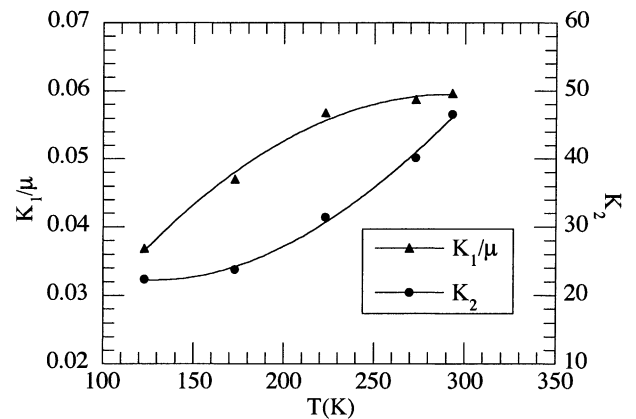

Fig. 4. Temperature dependence of the coefficients K_1/μ and K_2 of Eq. (4), $\dot{\varepsilon}_p = 2 \times 10^{-3}\,\mathrm{s}^{-1}$.

dependence suggests a direct correlation with that of the mean free path and annihilation rate. By decreasing the temperature, the flow stress increases strongly in this temperature regime. Thus, assuming that the microstructure at $\varepsilon_p = 0.01$ is independent of the testing temperature, the mean free path of the dislocations is expected to increase with the stress. As a consequence of the inverse dependence of K_1 on the mean free path, K_1 decreases with higher stress or equivalently by decreasing temperature. Note that a temperature dependence of K_1/μ was found Kocks in his original paper [17] for the 304 stainless steel while K_1/μ appeared to be rather insensitive to temperature for aluminium. The qualitative behavior of K_2 can also be understood as follows. The dynamic annihilation of dislocations can occur either by cross-slip of the screw segments owing to the strong elastic interaction between them or by climb of non-screw segments or by spontaneous annihilation when the attractive force between two dislocations on different planes exceeds the force required for dislocation climb [21,22]. This dynamic annihilation, regarded as a negative contribution to the strain-hardening, is in nature strongly thermally activated so that, qualitatively, K_2 is expected to increase with temperature.

We now focus on the initial stage of the strain-hardening, between $\varepsilon_p = 0.002$ and $\varepsilon_p = 0.01$, for the tensile curves obtained at $\dot{\varepsilon}_p = 2 \times 10^{-3}\,\mathrm{s}^{-1}$. Let us consider again the strain-hardening curve versus σ_{pl} in Fig. 3. While the strain-hardening decreases linearly above $\varepsilon_p = 0.01$, the early stage of strain hardening exhibits some curvature below $\varepsilon_p = 0.01$. This observation rules immediately out the possibility of reconstructing the entire stress–strain curve by connecting piecewise linked Voce curves. We have to search for an empirical function which, on the one hand, describes the curvature of $\theta_p(\sigma_{pl})$ below $\varepsilon_p = 0.002$ and on the other hand, which satisfies the continuity at $\varepsilon_p = 0.002$ and $\varepsilon_p = 0.01$, i.e. $\sigma_{pl}(\varepsilon_p = 0.002) = 0$ and $\sigma_{pl}(\varepsilon_p = 0.01) = \sigma_{0.01}$. A trivial empirical attempt is a function of the type

$$\sigma_{pl} = \sigma_{0.01}\left(\frac{\varepsilon_p - 0.002}{0.008}\right)^n \qquad 0.002 \leq \varepsilon_p \leq 0.01 \qquad (5)$$

where the coefficient n provides for the curvature. An example of application of the Eqs. (4) and (5) is presented in Fig. 5 where the fits through the experimental data of a tensile curve at 173 K are shown. Two separate fits have been calculated with the Eqs. (4) and (5), corresponding to the initial portion of the curve (below $\varepsilon_p = 0.01$) and from $\varepsilon_p = 0.01$ up to necking, respectively. Two different symbols have been used in the figure to distinguish between the low strain and high strain data. Let us emphasize that the use of Eq. (5) for this limited strain range is purely empirical and that it is a function with only one fitted parameter, namely n. Tests at five different temperatures, 293, 273, 223, 173 and 123 K, have been analyzed and very good fits have been systematically obtained. The temperature effect on Eq. (5) is reported in Fig. 6 where $\sigma_{0.01}$ is plotted along with the exponent n as a function of the temperature. From the tem-
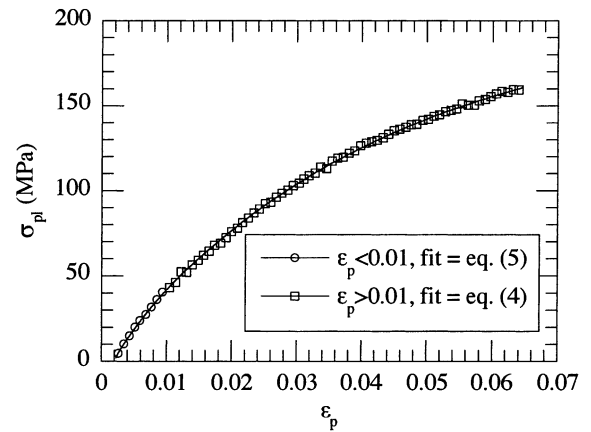

Fig. 5. Example of application of the fitting Eqs. (4) and (5) for $\sigma_{pl}(\varepsilon_p)$, $T = 173\,\mathrm{K}$, $\dot{\varepsilon}_p = 2 \times 10^{-3}\,\mathrm{s}^{-1}$.
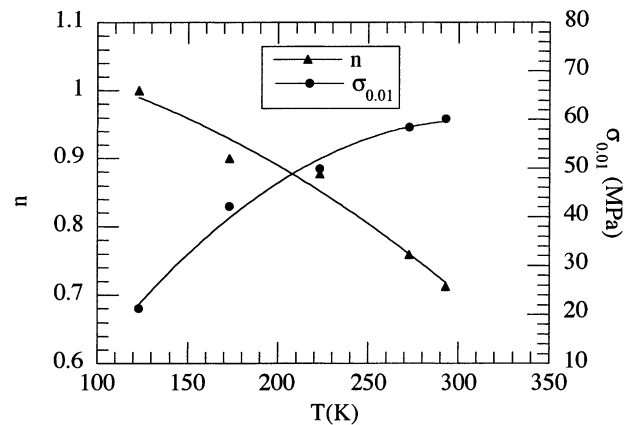

Fig. 6. Temperature dependence of the coefficients n and $\sigma_{0.01}(= \sigma(\varepsilon_p = 0.01) - \sigma_y)$ of Eq. (5), $\dot{\varepsilon}_p = 2 \times 10^{-3}\,\mathrm{s}^{-1}$.

perature dependence of n, it can be seen that the curvature of the curve $\sigma_{pl}(\varepsilon_p)$ decreases with decreasing temperature (n increases but smaller than 1) as observed for instance for the tensile curves presented in Fig. 1, while a significant decrease of $\sigma_{0.01}$ is observed. Moreover, at 173 K, $\sigma_{pl}(\varepsilon_p)$ has been assimilated to a linear function with $n = 1$.

Let us emphasize that the Eqs. (1)–(4) provide a basis for a further development of a model for the constitutive behavior of such steels, which is based on the micromechanics and dynamics of dislocations. The key parameters of the model are σ_y, $\sigma_{0.01}$, K_1, K_2 and n for which the temperature and strain-rate dependence can be determined. Obviously, more testing is necessary to obtain a series of equations describing the temperature and strain-rate dependence of these parameters.

4. Summary

An analysis of a series of tensile tests performed on a 8Cr ferritic/martensitic steel has been reported in this paper. An attempt to describe the overall stress–strain curves in the

limited strain range from the yield stress up to the necking has been done. First, the total flow stress has been separated into two major components, the yield stress and the hardening components. It has been shown that the yield stress is strongly thermally activated below room temperature and that the strain-rate dependence can be accounted for via a strain-rate compensated temperature. In order to derive the strain dependence of the hardening component, special attention has been paid to the strain-hardening behavior as a function of the stress. Two stages of strain-hardening have been identified, one for plastic strain smaller than 0.002 and one at higher strain up to necking. These two strain-hardening stages could be described by two simple mathematical relations. Moreover, in the second stage, the strain-hardening behavior has been found consistent with Kocks model which takes into account the storage and dynamic annihilation of dislocations. The deformation curves have been recalculated by connecting two fits corresponding to the two strain-hardening stages. Below room temperature, the temperature dependence of the strain hardening has been investigated and discussed. This dependence is contained in the four adjusted coefficients, $\sigma_{0.01}$, K_1, K_2 and n, of the fitting functions.

Acknowledgements

References

[1] D.S. Gelles, J. Nucl. Mat. 239 (1996) 99.
[2] A. Hishinuma, A. Kohyama, R.L. Klueh, D.S. Gelles, W. Dietz, K. Ehrlich, J. Nucl. Mat. 258-263 (1998) 193.
[3] M. Victoria, D. Gavillet, P. Spätig, F. Rezai-Aria, S. Rossmann, J. Nucl. Mat. 233-237 (1996) 326.
[4] D.S. Gelles, ASTM-STP 1047 (1990) 113.
[5] F. Abe, M. Narui, H. Kayano, Mat. Trans. JIM 34 (11) (1993) 1053.
[6] R.L. Klueh, J.M. Vitek, J. Nucl. Mat. 161 (1989) 13.
[7] G. R. Odette, K. Edsinger, G.E. Lucas, E. Donahue, ASTM-STP-1328, American Society for Testing and Materia, Philadelphia, PA, 1998, pp. 298–327.
[8] M. Tamura, H. Hayakawa, M. Tanimura, A. Hishinuma, T. Kondo, J. Nucl. Mat. 141-143 (1986) 1067.
[9] A.F. Armas, M. Avalos, I. Alvares-Armas, C. Petersen, R. Schmitt, J. Nucl. Mat. 258-263 (1998) 1204.
[10] R. Schäublin, P. Spätig, M. Victoria, J. Nucl. Mat. 258-263 (1998) 1178.
[11] P. Spätig, R. Schäublin, S. Gyger, M. Victoria, J. Nucl. Mat. 258-263 (1998) 1345.
[12] P. Spätig, G.R. Odette, G.E. Lucas, J. Nucl. Mat. 275 (1999) 324.
[13] P. Spätig, G.R. Odette, E. Donahue, G.E. Lucas, in: ICFRM9 Proceedings, J. Nucl. Mat., in press.
[14] P. Spätig, G.R. Odette, G.E. Lucas, M. Victoria, DOE Fusion Materials Semiannual Progress Report, DOE/ER-0913/26, 1999, p. 83.
[15] H. Mecking, in: A.W. Thompson (Ed.), Work Hardening in Tension and Fatigue, New York, Am. Inst. Min. Eng, 1977, p. 67.
[16] E. Voce, J. Instr. Met. 74 (1948) 537.
[17] U.F. Kocks, ASME J. Eng. Mater. Technol. 98 (1976) 76.
[18] K. Lücke, H. Mecking, in: R.E. Reed-Hill (Ed.), The Inhomogeneity of Plastic Deformation, 1973, p. 223.
[19] H. Mecking, K. Lücke, Acta Metall. 17 (1969) 279.
[20] U. Essmann, H. Mughrabi, Phil. Mag. A 40 (6) (1979) 731.
[21] J. Friedel (Ed.), Dislocations, Pergamon Press, London, 1964.
[22] U. Essman, M. Rapp, Acta Metall. 21 (1973) 1305.